Geologica Acta, Vol.5, Nº 1, 2007, 89-107
Available online at www.geologica-acta.com

geologica acta

The Impact of carbonate cements on the reservoir quality in the Napo Fm sandstones (Cretaceous Oriente Basin, Ecuador)

J. ESTUPIÑAN [1] R. MARFIL [1] A. DELGADO [2] and A. PERMANYER [3]

[1] Dpto. de Petrología y Geoquímica, Facultad de Geología, UCM
28040 Madrid, Spain. Estupiñan E-mail: jestupin@geo.ucm.es Marfil E-mail: marfil@geo.ucm.es

[2] Estación Experimental del Zaidín (CSIC), Laboratorio de isótopos estables
18008 Granada, Spain

[3] Dpt. de Geoquímica, Petrologia i Prospecció Geològica, Facultat de Geologia, Universitat de Barcelona
08028 Barcelona, Spain. E-mail: albert.permanyer@ub.edu

ABSTRACT

The Napo Formation of Lower-Middle Cretaceous age in the Oriente basin, Ecuador, is an important sandstone reservoir. The formation is buried at a depth of 1,500 m in the eastern part of the basin and down to 3,100 m in the western part. The sandstones display higher porosity values (av. 20%) than other reservoirs in the region. These sandstones were deposited in fluvial, transitional and marine environments, and they are fine to medium grained quartzarenites and subarkoses. The principal cements are carbonates, quartz overgrowth and kaolin, with scarce amounts of pyrite-pyrrhotite and chlorite. Carbonate cements include: Eogenetic siderite (S1), mesogenetic and post-compactional calcite, Fe-dolomite, ankerite and siderite (S2). Early siderite and chlorite helped to retain porosity by supporting the sandstone framework against compaction. Dissolution of feldspars and carbonate cements are the main mechanism for secondary porosity development during mesodiagenesis. The high intergranular volume (IGV) of the sandstones indicates that cementation is the predominant contributor to porosity loss in the reservoir and that the precipitation of the carbonate cement occurred in early and late diagenetic stages. The stable–isotope composition of the S1 siderite is consistent with precipitation from meteoric waters in fluvial sandstones, and from mixed meteoric and marine waters in transitional sandstones. The low $\delta^{18}O‰$ values of some of these carbonate phases reflect the replacement and recristalization from S1 to S2 siderite at deep burial and high temperature. Textural evidence, together with a low Sr content, also suggests that siderite (S1) in fluvial environment is an early cement that precipitated from meteoric waters, near the sediment/water interphase, followed by the generation of calcite with a higher Fe and Mg content. However, due to this higher Mg content, siderite S2 could have precipitated as a result of the thermal descarboxilation of the Mg rich organic matter. The progressive decrease in $\delta^{18}O$ values in all carbonate cements could be related to the continued precipitation at different temperatures and burial depth.

KEYWORDS | Carbonate cement. Geochemistry. Sandstone reservoirs. Oriente Basin. Ecuador.

INTRODUCTION

The most important oil reservoirs in Ecuador are found in the Oriente Basin (Fig. 1). The sandstones of the Hollín and Napo Fms (Fig. 2) of Cretaceous age contain the largest hydrocarbon reserves. Analyses related to the diagenesis effect on these reservoir sandstones are scattered. A complete petrological and geochemical study including diagenetic processes, isotopic analyses of the carbonate cements, as well as a general diagenetic sequence of the principal events, would improve and optimise hydrocarbon recovery production.

The spatial distribution of diagenetic alterations in fluvial, transitional and marine sediments is strongly influenced by sea-level changes, depositional facies and the extent of mixing between marine and meteoric waters (Morad et al., 2000). Likewise, the burial depths at which the mesogenetic reactions occurred may vary considerably depending on the burial-thermal history of the sequence.

The purpose of this study is to investigate the diagenetic history of the reservoir sandstones of the Napo Fm, as well as to discuss the distribution of the carbonate cements and their possible relation to the depositional environment or with the fluids that circulate at burial depth. The study also includes the relationship between the preservation of primary porosity and the generation of secondary porosity. A combination of optical microscopy, CL and SEM, as well as geochemical (microprobe and stable isotopic) analyses were used in order to provide detailed constraints on the diagenetic sequence, the evolution of pore fluid composition, and the relative timing of carbonate cement precipitation.

GEOLOGICAL SETTING

The Oriente Basin is part of a major morfo-structural unit called the Upper Amazon Basin which comprises parts of Colombia, Ecuador, Peru, Bolivia, and Brazil. The structure of the basin is the result of transpressive stress from the Upper Cretaceous deposits which produced the uplift of the Cordillera Real and the formation of the back-arc basin. Nevertheless, a previous stage of oil-bearing process existed which was of fundamental importance. It began in the Turonian age with compressive stress that marked the tectonic inversion developed in the Permo-Triassic and Jurassic periods. During this tectonic inversion, the whole oil structure of the basin developed (Baldock, 1982; Dashwood and Abbotts, 1990).

The Hollín, Napo and Basal Tena formations, located at the east of the Andes Cordillera, belong to the Cretaceous period in the Oriente Basin. The oil reservoirs studied correspond to the Napo "U" and "T" sandstones (Upper Albian – Upper Cenomanian; Fig. 2). They are characterised by cyclic sequences of limestone, shale, and sand-

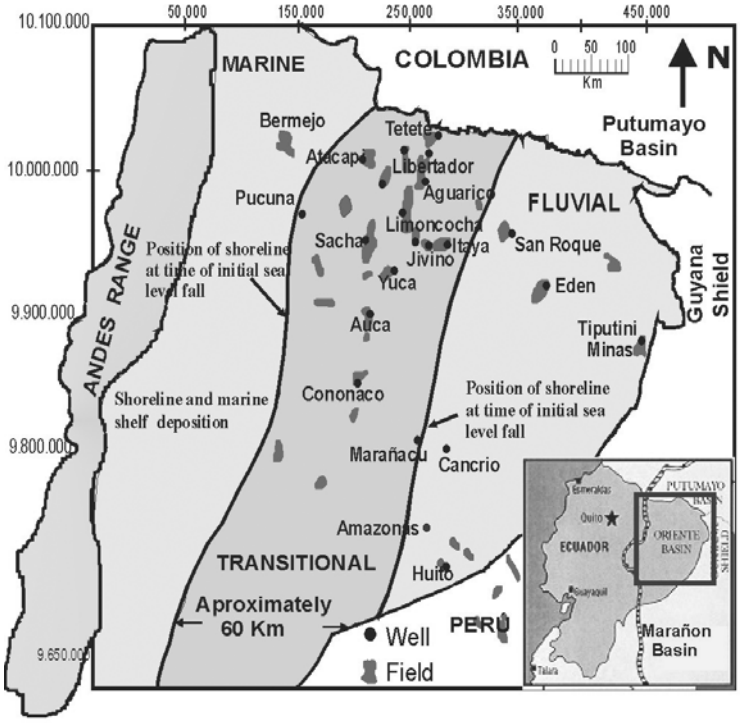

FIGURE 1 | **Location, distribution and paleogeographical map of the Napo Formation showing the shoreline at the maximum sea level fall and the initial sea level fall. The black dots show the sampled wells (adapted from White et al., 1995).**

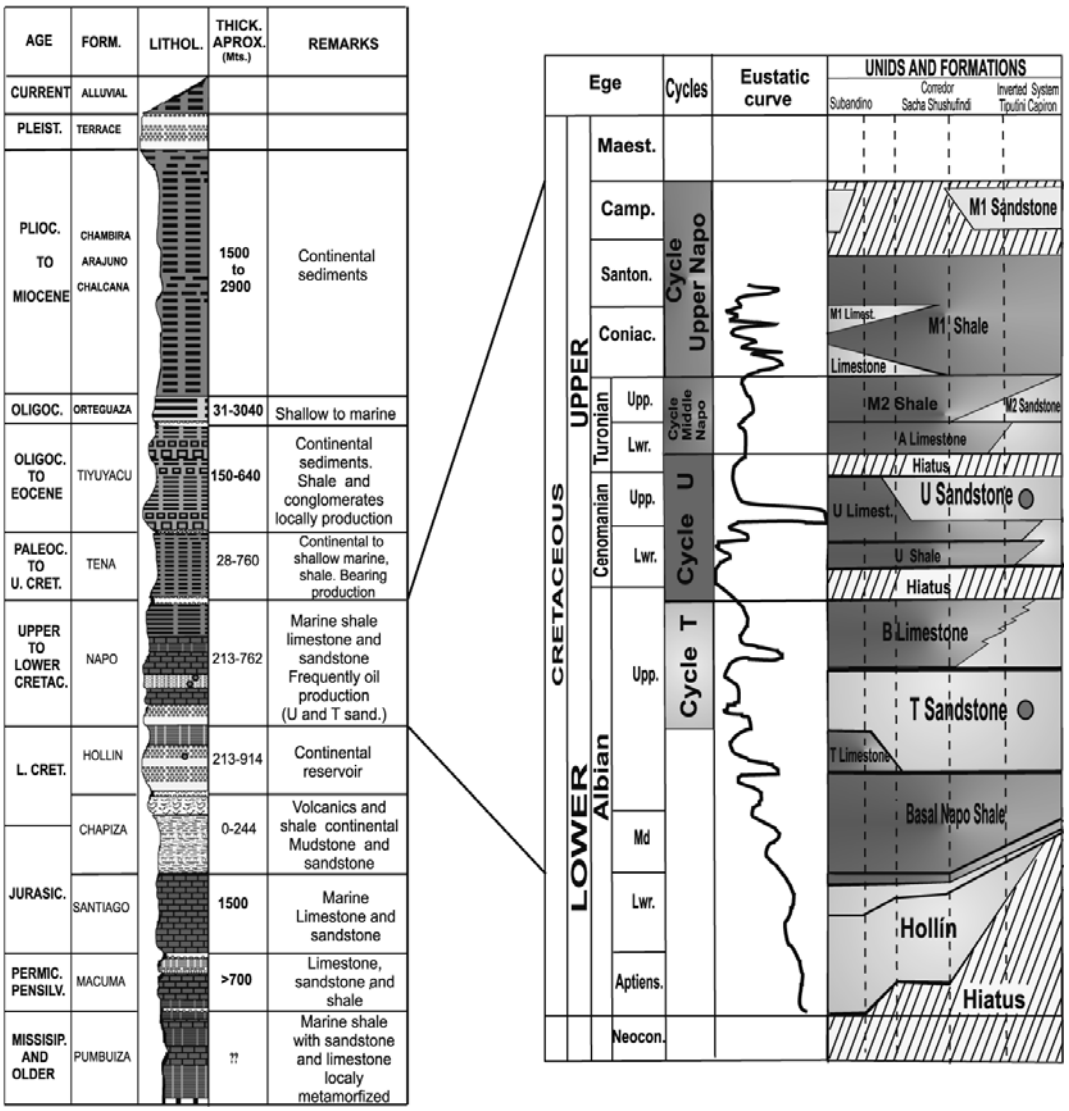

FIGURE 2 | **General stratigraphical column of the Oriente Basin with lithostratigraphic nomenclature (modified from Almeida, 1986). Detailed chart showing the reservoirs "U" and "T" sandstones from the Napo Formation [after Christophoul and Rivadeneira (1986)] modified from Jaillard, 1997).**

stone, whose deposition and distribution were controlled by relative changes in the sea level (White et al., 1995; Fig. 2).

The Napo Fm age is between Aptian and Campanian and was deposited over a stable sea platform in a passive margin with low subsidence. Seismic interpretation and data from the wells show the complex structural history of the Oriente Basin, where extensional and compressional events occurred. The recent structures were influenced by previous tectonic events that took place during Precambrian and Lower Palaeozoic. In the Lower Cretaceous a regional compression affected the entire basin. In the Eastern part some faults were inverted and erosion produced an unconformity during the Aptian.

The interval of the studied sandstones represent two cycles of regression and transgression. The boundaries of the sequences at the base of the reservoir are erosional events associated with the fall of the sea level during the Upper Albian and Cenomanian. As the sea level began to rise again, facies from the estuary and nearshore were deposited in the incised valleys (Fig. 1).

SAMPLING AND METHODS

The well samples studied from the Napo "U" and "T" sandstones were taken from a depth of 1459 m to 3123 m where the formation temperature ranges from 80 to 110ºC. Fifty four samples of the cored intervals from 22 wells were selected. After eliminating oil from the porosity, the samples were impregnated with blue-stained resin and then ground deeply enough to avoid artifact porosity. Thin sections were stained for feldspar and carbonates. Quantification of mineralogy and porosity was performed by counting 300 points per thin section. A standard petrographic microscopic Zeiss (Axioskop) with x2.5, x10, x20, x40 lenses was used. Cathodoluminescence (CL) observations were performed using "cold" Technosyn 8200 Mk 4 models connected to an Olympus BHA-P microscope with 4x and 10x magnifying lens. The conditions for the observation were 11-16 Kv volt-

age, with an intensity of 300-500 μA and 0.2-0.1 Torr of vacuum. Mineralogy was confirmed by X- ray diffraction, using a Philips PW 1720 diffractometer equipped with Cu(Kα) radiation. The data were processed with the Philips APD program. To determine the textural relationship between the cements and clay minerals, we used a scanning electron microscope (SEM) model JEOL JSM 6400 equipped with an energy–dispersive X-ray microanalyzer in secondary electron and backscattered electron modes (BSE).

Thirteen representative samples were selected for the carbonate cements analyses. Their chemical compositions were determined by microprobe analyses. Ninety eight analyses corresponding to the Napo "U", and 192 to Napo "T" sandstone, were performed. A JEOL JXA–8900 model (15 Kv accelerating voltage, 2.147E-08 A beam current, 5 μm beam size, 100 % ± 3.5% total accepted) was used. Detection limits are approximately 100 ppm for Mg, 250 ppm for Mn and 300 ppm for Fe. The BSE system of the microprobe was used for detection of zonation. For all cements, results were normalized to 100 mol% $FeCO_3$, $MnCO_3$, $MgCO_3$, $CaCO_3$ and $SrCO_3$.

Oxygen and carbon isotopic compositions of the carbonate cements were determined at the Experimental Station of Zaidín (CSIC) Granada, using a Finnigan MAT 251 mass spectrometer. The samples containing more than one phase of cement were separated after the treatment for the chemical sequential (Al-Aasm et al., 1990). The isotope values were obtained in ‰ and the isotopic relation from the oxygen and carbon referent to the standard (V-PDB).

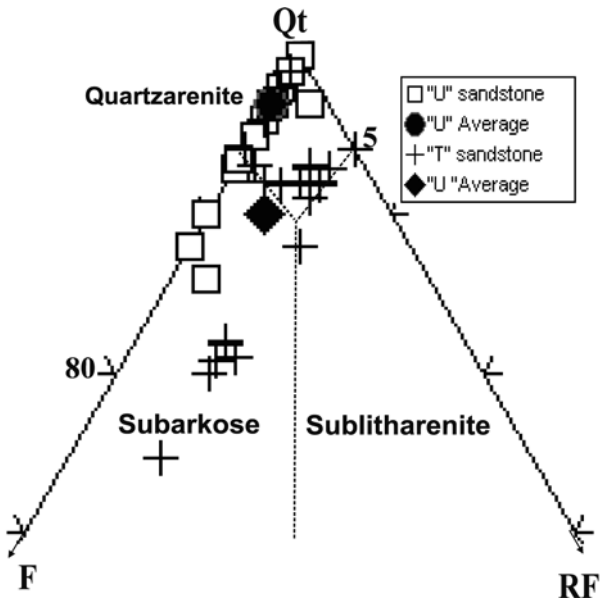

FIGURE 3 | **Detrital composition of representative sandstones from the Napo Formation, plotted on Qt-F-RF (Dott, 1964 and modified by Pettijohn, 1972). Abbrevations: Qt: Quartz; F: Feldspar; RF: Rock fragments.**

SANDSTONE PETROGRAPHY

Napo "U" sandstones have a rather uniform composition in terms of quartz, feldspar and rock-fragments, being quartzarenites with a few subarkoses. The average composition is $Qt_{96.5}\ F_{3.1}\ Lt_{0.4.}$ Napo "T" sandstones, on the other hand, are subarkoses, with an average composition of $Qt_{89.8}\ F_{6.8}\ RF_{3.1}$ (Fig. 3). In general all the sandstones are fine to coarse grained, with moderate to good sorting, and round to subround grains, including some angular and subangular subordinated grains. The argillaceous matrix is scarce (< 1 %).

Modal analyses reveal that the most common detrital component is quartz, dominantly monocrystalline in relation to the polycrystalline quartz grains (Tables 1 and 2). Zircons and minor tourmaline amounts are frequently included in the monocrystalline quartz. Chert occurs in trace amounts. Rock fragments are igneous (volcanic), metamorphic (quartzite), and scarce sedimentary rocks (< 2%). The detrital quartzs are corroded by the carbonate cements. K-feldspar dominates over plagioclase in all depositional facies and they vary between 0-7%. These feldspars are occasionally replaced by carbonates and in some cases, albitized. Most of the feldspar grains show evidence of dissolution. Micas (biotite and muscovite), zircons and tourmaline are only minor constituents in the sandstones (av. 0-2%). The intrabasinal components are glauconite and phosphatized micritic grains.

Besides the carbonate cements, there are other fairly abundant cements such as quartz overgrowths (av. 16%) and pyrites-pyrrhotite (av. 2%). Kaolin occur as *pore-filling* and epimatrix, (av. 0–7.3%). Dickite is distinguished from kaolinite by SEM and XRD analyses. Dickite crystals show no etching and are much thicker (5-10 μm) than the kaolinite which postdates the quartz overgrowth and the carbonate cements. Chlorite appears as *rims* (av. 3%) composed of platelets oriented perpendicularly to the grain surface.

PETROGRAPHY AND CHEMISTRY OF CARBONATE CEMENTS

Postdepositional processes resulted in a quite significant modification of depositional porosity. In addition to compaction, quartz, carbonate and clay mineral cementation are the major porosity reducing factors. Carbonate cements occur in the hydrocarbon reservoir of the Napo Fm. They include: siderite, calcite, dolomite-Fe and ankerite phases (Tables 1 and 2).

Siderite

Two siderite cement generations were distinguished. Siderite (S1) occurs as small lenticular crystals (10–50 μm)

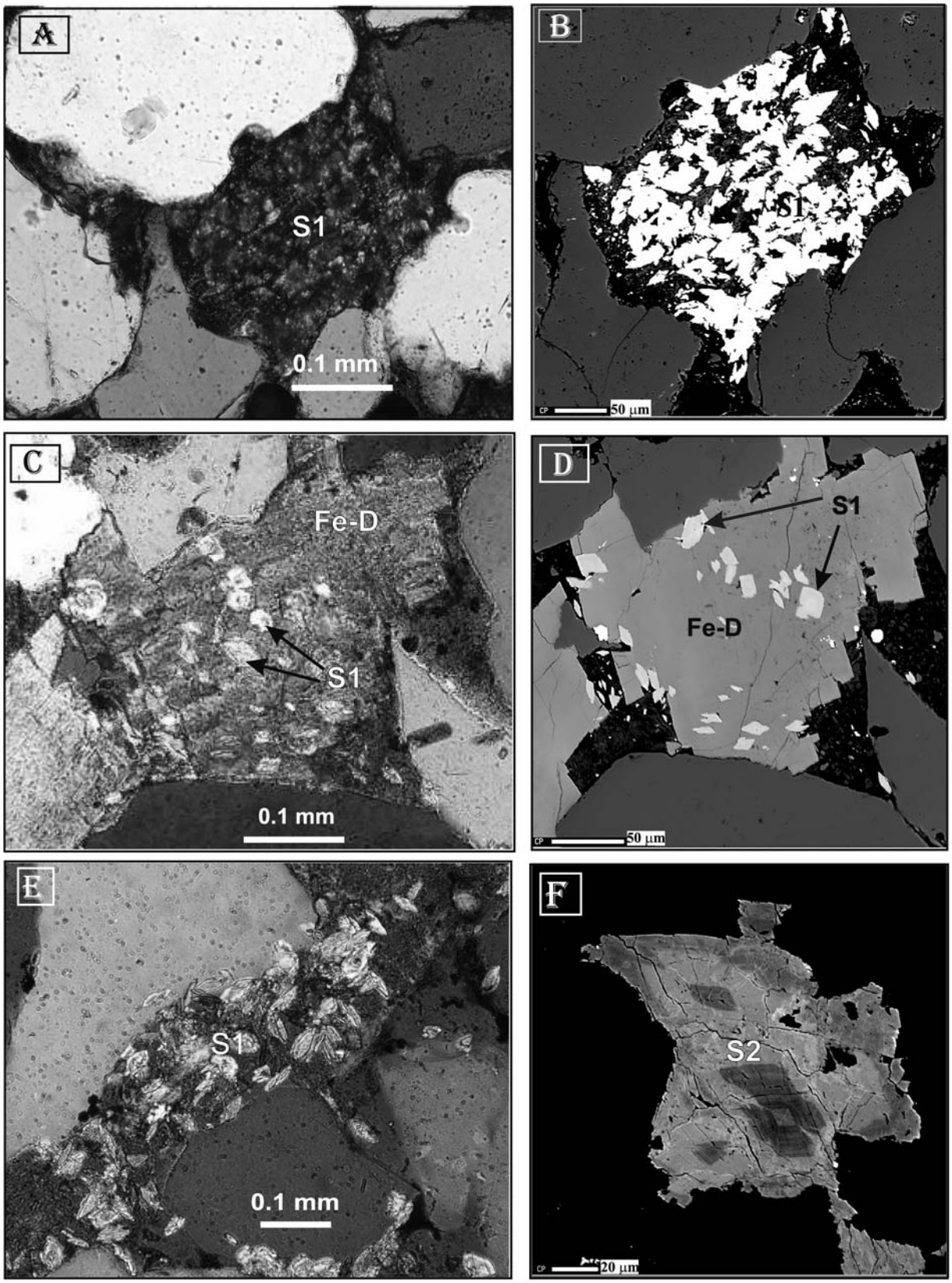

FIGURE 4 | **Petrographic aspects of siderite cements. Left: optical photomicrograph. Right: BSE images. A and B) Thin lens crystals of siderite (S1) replacing feldspar. C and D) Fe-dolomite engulfing siderite lens and small rhombs (S1). E) Optical photomigraph. Petrography aspects of siderite (S1) corroding quartz grains and replacing clay intraclast. F) BSE image of siderite (S2) showing zonation with higher Mg content in the core and outer zone.**

TABLE 1 | **Representative modal analysis of the "U" sandstones from the Napo Formation.**

U	MARINE	TRANSITIONAL											FLUVIAL				
depth (ft)	PC-2 9374'	AA-10 9192,5'	AT-2 9402'	CN-4 9988'	IY- B6 p Av. n= 7	JV-1 Av. n= 2	JV-3 Av. n = 4	LM-9 9435'	SC-126 9431'	TT-1 9026'	YC-2 9549'	Average TRANSITIONAL	ED-10 7365'	MR-1 8958,2'	TM-1 4787'	Average "FLUVIAL"	Average "TOTAL U"
	%	%	%	%	%	%	%	%	%	%	%		%	%	%		
Qmr	32.6	31.8	44.30	34.6	39.6	38.0	38.2	38.6	36.0	40.0	34.3	37.5	35.3	36.7	40.7	37.6	35.9
Qmo	6.7	5.3	6.67	10.0	8.0	14.0	10.2	9.3	7.0	7.5	12.4	9.0	11.0	10.0	4.7	8.6	8.1
Qp2-3	6.0	11.3	6.67	8.3	5.0	3.8	7.4	7.0	4.4	10.7	9.7	7.4	5.0	4.7	3.3	4.3	5.9
Qp >3	1.7	3.0	2	2.7	1.0	1.8	2.6	0.3	1.0	1.3	3.7	1.9	2.0	0.9	1.0	1.3	1.6
Q fr.met.		0.0		0.0	0.3	0.2	0.25	0.3	0.3			0.1	0.3	0.0	0.3	0.2	0.1
K-F	0.7	0.7	1.3	1.0	2.0	2.0	0.5	0.7	2.3	0.3		1.1	6.7	0.0	2.3	3.0	1.6
CO3-KF	0.7	1.30	0	1.3	0.2				0.0		0.0	0.3		0.7	3.7	1.4	0.8
Plg + Alb		0.0	0.3	0.7	0.8	0.3	0.1		1.4		0.7	0.4		0.7	1.4	0.7	0.4
Chert	0.0				0.3		0.1	0.3				0.1			0.0	0.0	0.0
Opaques	0.3		0.7			0.8	1.6	0.7	4.3		0.0	0.8		0.0	0.0	0.0	0.4
Muscovite		1.0		0.3	0.3	0.2					1.0	0.3	1.0		0.0	0.3	0.2
Biotite		0.0			0.3			0.3				0.1	0.0			0.0	0.0
Heavy minerals		0.2				0.1				0.1	0.1	0.1	0.6	0.3		0.3	0.1
Total	48.6	54.7	61.9	58.9	57.8	61.3	60.9	57.5	56.7	59.9	61.9	59.2	61.9	53.9	57.4	57.8	55.2
Quartz	12.0	15.0	18.10	10.0	15.0	14.0	16.0	17.0	7.0	14.0	9.0	13.5	11.0	10.0	12.0	11.0	12.2
Calcite	2.00			1.0	0.2		0.3					0.2		21.0	1.0	7.3	3.2
Fe-dolomite/ankerite	10.66	2.00							14.70			1.7			1.67	0.6	4.3
Siderite	2.4		0.00		0.0			0.4	0.0	0.7		0.1		0.0	3.0	1.0	1.2
Kaolin	0.0	3.3	3.70	2.0	2.8	3.0	5.0	6.7	1.3	4.0	3.0	3.5	2.1	0.0	0.3	0.8	1.4
Pyrite	0.7	0.7		0.7	0.3	0.8			0.0	0.0	0.0	0.2		2.3		0.8	0.6
Chlorite	0.0	2.7	0.00	1.0	0.0	1.0			0.0	0.0	0.7	0.5	1.0	0.0	0.0	0.3	0.3
Total cement	27.7	23.7	21.8	14.7	18.3	18.8	21.3	24.1	23.0	18.7	12.7	19.7	14.1	33.3	18.0	21.8	23.1
Epimatrix	3.3	7.0	2.3	6.3	2.8	0.2	0.4	2.0	2.0	4.0	6.0	3.3	1.7	0.3	1.3	1.1	2.6
Pseudomatrix		1.0		1.0		1.0	0.3	0.3	0.3		1.6	0.5	0.7			0.2	0.3
Total	3.3	8.0	2.3	7.3	2.8	1.2	0.7	2.3	2.3	4.0	7.6	3.8	2.4	0.3	1.3	1.3	2.8
Glauconite	5.7	1.0	0.6	0.1		0.2			0.3		0.1	0.2	0.3	5.7		2.0	2.6
P1 porosity	9.0	5.7	8.3	11.7	13.1	10.6	14.3	14.4	16.0	13.4	7.0	11.5	13.3	4.7	13.3	10.4	10.3
P2 porosity	5.7	7.0	5.1	7.3	7.9	7.9	2.8	1.7	1.7	4.0	10.7	5.6	8.0	2.0	10.0	6.7	6.0
(P1+P2)	14.7	12.7	13.4	19.0	21.0	18.5	17.2	16.1	17.7	17.4	17.7	17.1	21.3	6.7	23.3	17.1	16.3
Total	100.0	100.0	100.0	100.0	100.0	100.0	100.0	100.0	100.0	100.0	100.0	100.0	100.0	100.0	100.0	100.0	100.0
Grain size	Fu - Fl	Fu-mu	fl-ml	fu-ml	fu-ml	fu-ml	Fu-ml	fu-fu	Fl-fl	fl-ml	fu-ml		mu-Crsl	Fu-ml	Fl-fu		
Sorting	good	Mod.	good	mod	good	good	good	good		good	mod		good	good	mod.		
IGV	36.80	38.00	35.80	32.33	35.52	34.80	37.16	38.40	37.70	33.70	28.00	35.1	31.33	39.67	36.33	35.8	35.9
COPL	5.00	3.30	6.6	11.33	6.95	7.90	3.90	2.60	3.60	9.50	15.90	7.2	6.70	1.60	5.80	4.7	5.6
CEPL	23.60	24.50	20.9	15.40	20.85	16.60	19.70	21.70	21.20	16.90	10.70	18.8	16.40	33.40	19.10	23.0	21.8
ICOMPACT	0.12	0.10	0.2	0.38	0.25	0.23	0.20	0.10	0.07	0.31	0.63	0.2	0.45	0.02	0.26	0.2	0,2

TABLE 2 | **Representative modal analysis of the "T" sandstones from the Napo Formation.**

	MARINE			TRANSITIONAL											FLUVIAL						
Arenisca "T"	PC-2	AA.-10	AC-16	CN-4	CN-4	IT- B-6	JV-1	JV-3	LM-9	SC-99	SC-105	SC-126	YC-2	YB-1	**Average**	AZ-1	CR-1	ED-10	HT-1	S RQ-1	Average	Average
Prof. (ft)	9623	9412,0	9976,0	10248'	10249,0	Av.	9500,0	9492,0	9699,0	9649,0	9757,0	9670,0	9791,0	9829'	**Transitional**	9663,0	8863,0	Av.	9488,0	Prom.	fluvial	Total
	%	%	%	%	%	nº = 5	%	%	%	%	%	%	%	%		%	%	nº = 4	%	nº = 2		
Qmr	36.0	27.7	32.3	31.9	22.0	38.1	32.0	26.7	35.0	33.6	32.4	32.3	31.4	37.0	31.7	27.2	23.0	30.0	29.0	34.6	28.8	32.2
Qmo	3.0	10.3	10.0	5.0	6.3	6.6	11.0	3.0	5.0	7.4	6.7	4.0	6.1	8.2	6.9	4.7	10.0	6.0	6.0	4.3	6.2	5.4
Qp2-3	6.0	10.0	6.3	5.7	2.3	8.0	7.0	5.3	4.3	5.3	5.0	8.3	3.0	2.4	5.6	3.7	5.7	5.0	3.3	6.7	4.9	5.5
Qp>3	0.7	1.7	1.3	0.7	0.7	1.6	1.0	3.0	2.0	1.7	1.7	0.3	1.4	1.7	1.4	1.3	3.0	3.0	2.0	1.0	2.1	1.4
Q fr.met	1.0	1.0	0.0	0.7	0.7	0.0	0.0	1.0	0.7	0.3	0.0	0.3	0.0	0.0	0.4	0.3	0.3	0.3	0.7	0.2	0.4	0.6
K-F	1.0	0.0		0.0	0.0	1.0	0.3	5.0	1.0				0.3	1.0	1.0	1.2	1.4	3.0	1.7	0.0	1.5	1.1
CO3-KF	2.6	0.0	0.0	0.0	0.0		0.0	0.0	1.0	0.0	0.0	0.0	0.3	0.0	0.1	0.0	0.0	0.0	2.3	0.0	0.5	1.1
Plg +Alb.	2.0	2.0	3.0	4.0	4.6	0.7	3.0	0.0	1.7	1.7	0.6	2.6	1.0	1.0	2.0	4.0	4.9	0.1	4.5	1.8	3.1	2.4
Opaques	1.3	3.2	3.0	1.0	2.0	1.8	1.0	1.0	1.3	3.7	0.0	4.0	1.0	1.0	1.8	1.0	0.3	1.0		2.0	1.1	1.4
Muscovite	0.0	0.3	0.3	0.5	1.7	0.0	0.3	1.0	0.0	1.0	1.0	1.0	2.0	2.4	0.9	0.3	0.3	1.0		1.0	0.7	0.5
Biotite	0.0	0.3		0.4	1.3	0.0	1.0	0.0	0.0	0.3				0.3	0.4	0.3	1.0	0.1	0.0	0.0	0.3	0.2
Heavy minerals	0.0		0.7	0.3	0.3				1.0	1.4	1.6	0.0		0.7	0.7	2.0		0.1		1.0	1.0	0.6
Total	53.6	56.6	57.0	50.1	41.9	57.8	56.7	46.0	53.0	56.4	48.9	52.9	46.6	55.8	52.3	46.1	50.0	49.7	49.5	52.6	49.5	51.8
Quartz	19.0	17.3	17.0	16.3	17.0	17.4	15.7	14.0	23.0	16.0	19.0	16.3	12.2	16.1	16.7	16.4	16.0	23.0	24.2	16.0	19.1	18.3
Calcite	2.0	0.8	0.7	4.7	3.3				2.0	2.0	1.0		3.0	2.4	2.2	2.0	1.7	2.0		0.5	1.5	1.9
Fe-dolomite/ankerite	3.0	1.0			0.0		0.7		1.0			2.0	1.0	4.1	1.4	5.0	4.0	1.0		1.0	2.8	2.4
Siderite	2.0	3.0	1.0	2.7	3.3		3.7	3.9	1.3	5.0	2.0		2.0	1.7	2.7	3.0	1.0	1.0	1.0	1.0	1.4	2.0
Kaolin	2.3	6.7	1.7	2.3	6.7	3.0	5.0	0.0	1.7	2.7	4.3	5.7	8.0	3.4	3.9	1.5	3.3	3.3	1.0	5.0	2.8	3.0
Pyrite	0.0	0.0		0.3	1.0	1.0	0.0	1.3	0.0	0.3	0.3	0.0	3.0	0.0	0.6		0.3	0.1		0.2	0.2	0.3
Chlorite	0.0	1.0	0.0	0.7	2.7	0.1	1.0	0.0	0.0	0.0	0.0	1.1	4.1	1.0	0.9	0.0	2.3	0.2	0.3	0.6	0.7	0.5
Total cement	28.3	29.8	20.3	27.0	34.0	21.5	26.0	19.2	29.0	26.0	26.7	25.1	33.3	28.8	26.7	27.9	28.7	30.7	26.5	24.2	27.6	27.5
Epimatrix	1.7	1.0	2.0	3.2	5.7	1.1	1.3	0.7		1.3	3.1	4.3	1.6	0.0	2.1	3.0	6.3	0.2	0.3	3.7	2.7	2.2
Pseudomatrix		0.0	0.0	0.0	0.7		0.0			1.0	0.6	0.3	0.0	0.0	0.3	1.0	0.0	0.1	0.7	0.5	0.5	0.2
Total	1.7	1.0	2.0	3.2	6.4	1.1	1.3	0.7	0.0	2.3	3.7	4.6	1.6	0.0	2.1	4.0	6.3	0.3	1.0	4.2	3.2	2.3
Glauconite	0.0	0.0	0.7	0.0	0.7	0.1	0.3	16.7	0.0	0.3	0.7	0.0	0.0	3.4	1.8	7.3	0.0	0.0	12.0	0.3	3.9	1.9
P1 porosity	13.7	10.0	15.7	14.3	9.7	16.0	9.0	12.3	16.7	11.0	15.0	16.7	16.9	9.9	13.3	11.7	9.0	12.4	10.0	15.9	11.8	12.9
P2 porosity	2.7	2.7	4.3	5.3	7.3	3.5	6.7	5.0	1.3	4.0	5.0	0.7	1.7	2.1	3.8	3.0	6.0	6.9	1.0	2.9	3.9	3.5
P1 + P2	16.4	12.7	20.0	19.7	17.0	19.5	15.7	17.3	18.0	15.0	20.0	17.4	18.6	12.0	17.1	14.7	15.0	19.3	11.0	18.7	15.7	16.4
Total	100.0	100.0	100.0	100.0	100.0	100.0	100.0	100.0	100.0	100.0	100.0	100.0	100.0	100.0	100.0	100.0	100.0	100.0	100.0	100.0	100.0	100.0
Grain size	Fl - Fu	Fu-mu	Fl - Fu	Fl -Fl	Fl -Fl	Fu-mu	Fl -Fu	Fl -Fu	Fl - Ml	Fu - Fl	Fu -Ml	Fl - Fu	Fl	Fu - Fl		Fu- Crsl	Fu-crsl	Fu- Crsl	Fu -Mu	Fu-mu		
Sorting	good	good	good	good	good	good	good	good	good	good	good	good	poor	good		mod.	mod.	good	good	mod		
IGV	36.30	29.00	36.60	36.70	36.70	37.50	31.7	32.0	35.3	31.70	39.00	35.30	35.70	31.00	34.5	30.30	31.00	34.60	36.30	32.10	32.9	34.5
COPL	5.8	15.50	5.30	5.26	5.30	4.60	12.2	11.8	7.2	12.2	1.60	7.20	6.7	13.0	8.3	13.90	13.90	8.20	5.80	11.70	10.7	8.3
CEPL	18.80	13.80	15.80	16.10	18.80	16.90	14.20	12.90	17.00	14.00	18.70	16.70	16.20	16.80	16.0	13.50	13.50	16.60	23.20	14.20	16.2	17.0
ICOMPACT	0.20	0.50	0.20	0.20	0.20	0.22	0.40	0.50	0.30	0.50	0.10	0.30	0.30	0.40	0.3	0.50	0.40	0.30	0.20	0.50	0.38	0.3

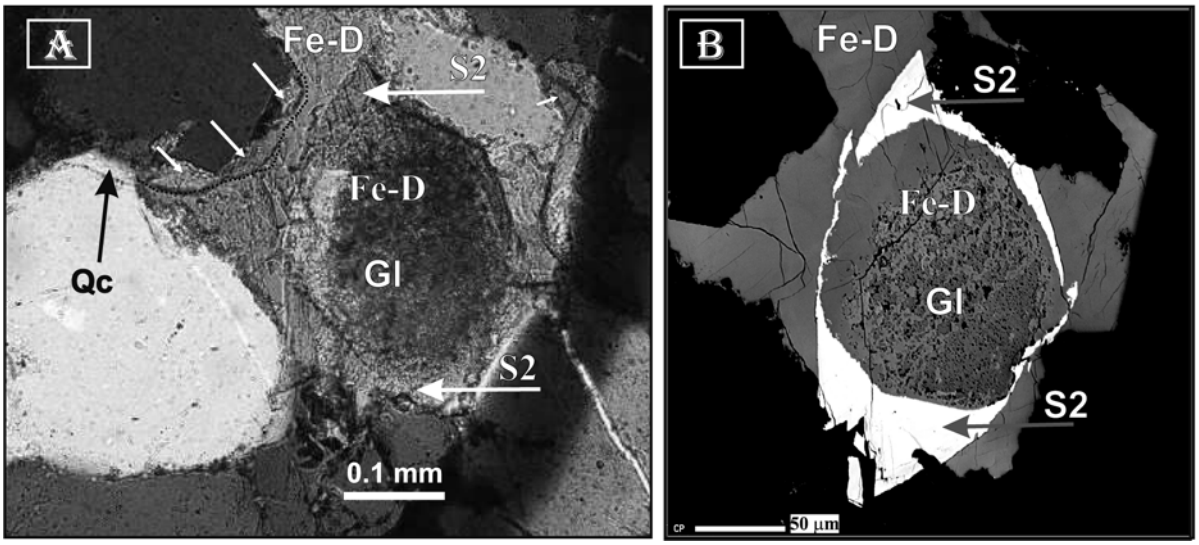

FIGURE 5 | **A and B) Fe-dolomite replacing glauconite and preceding the overgrowth development of S2 siderite. Fe-dolomite and S2 siderite are post quartz overgrowth (see arrows).**

and as euhedral rhombs that fill intergranular pores and in some case, replaces feldspars and clay intraclasts (Figs. 4A to 4E). Siderite (S2) occurs as large rhombic crystals (Fig. 4F), which partially replace dolomitized glauconite (Figs. 5A and 5B). Under CL, siderite S1 is not luminescent but S2 shows orange luminescence. S1 cement is partially replaced by Fe-dolomite (Figs. 4C and 4D), calcite or ankerite. Siderite cement forms 5% of the total volume of all the analysed samples. Siderite (S1) pre-dates quartz cement, as is shown under optical microscope and SEM observations. However, the quartz overgrowth shows corrosion or embayment by S2 siderite. S1 siderite cement appears in all sandstones and S2 only in transitional and marine sandstones from Pucuna, Yuca and Jivino (Fig. 1)

The average composition of siderite (S1) is ($Fe_{81.8}$ $Mg_{10.2}$ $Mn_{0.9}$ $Ca_{7.1}$)CO_3, (Table 3). Some samples have values up to 99% of $FeCO_3$, and a high content in Mn (>3.9). The average composition of S2 siderite is ($Fe_{67.8}$ $Mg_{20.5}$ $Mn_{0.8}$ $Ca_{11.1}$) CO_3 (Table 3). These cements are zoned in terms of Mg which is higher in the core than in the outer zone (Fig. 4F). The average compositions of siderites S1 and S2 are similar except for low Mn content (< 1%) and the high Mg of the S2 (Table 3, and Figs. 6 and 7). Another characteristic of the marine sandstones is the presence of glauconite partially replaced by S2 siderite and later replaced by Fe-dolomite (Figs. 5A and 5B).

The $\delta^{13}C$ ‰ PDB values in Napo "U" sandstones vary between -3.2 and -10‰, and $\delta^{18}O$ between -3.2 and –11.4‰ PDB (Table 3). The $\delta^{13}C$ ‰ PDB in "T" sandstones vary from -2.4 to -9.6 ‰, and $\delta^{18}O$ from -3.0 to -13.8 ‰ PDB (Table 3). These data correspond to (S1+S2). Likewise, we have selected under BSE the richest samples in S1 or S2, in order to separate both phases in the isotopic plot.

Calcite

Calcite cement is scarce in the fluvial sandstones and the average content is 5% of the total volume (Tables 1 and 2). Calcite appears as sporadic patches (up to 80 µm), poikilotopic texture of 50–100 µm (Figs. 8A and 8B) with no luminescence or red orange luminescence. Calcite replaces feldspars (Figs. 8C and 8D). Calcite cement appears as

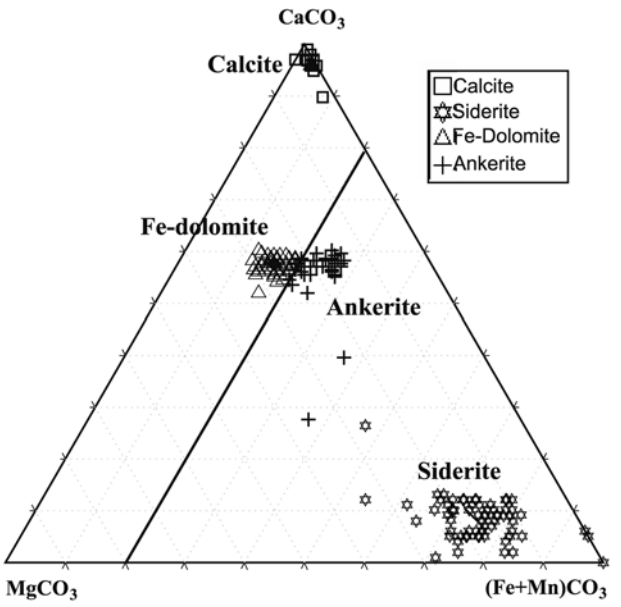

FIGURE 6 | **Chemical composition of representative carbonate cements (Ca, Fe+Mn, Mg)CO_3, from the Napo Formation.**

TABLE 3 | **Chemical composition from microprobe analyses and isotopic ratios of representative carbonate cements in the Napo Formation.**

sandstone Samples	MARINE CO_3 Mg	Ca	Mn	Fe	Sr	TRANSITIONAL CO_3 Mg	Ca	Mn	Fe	Sr	FLUVIAL CO_3 Mg	Ca	Mn	Fe	Sr	$\delta^{13}C$ (‰ V-PDB)	$\delta^{18}O$ (‰ V-PDB)	Remarks
"U" Sandstone																		
SIDERITE S1																		
average	18.6	11.6	0.9	69.1	0.0						12.4	9.2	0.9	77.5	0.0	-3.4	-3.7	Siderite lens
maximum	19.3	12.2	0.7	70.5	0.0						13.9	10.9	1.0	80.0	0.0	-3.6	-4.3	
minimum	17.8	11.0	0.6	67.8	0.0						11.2	7.0	0.7	75.4	0.0	-3.2	-3.2	
SIDERITE S2																		
average	23.8	13.9	0.4	61.8	0.0											-8.5	-10.8	Rhombic siderite
maximum	27.6	27.0	0.8	66.5	0.0											-10.0	-11.4	Occasionally zoned
minimum	20.7	8.0	0.2	45.8	0.0											-7.1	-10.3	
CALCITE																		
average	3.8	96.5	0.1	0.5	0.1						1.3	95.4	1.0	2.3	0.0	-3.5	-11.4	poikilotopic calcite
maximum	4.0	97.0	1.3	0.9	0.1						1.9	97.6	1.3	3.1	0.0	-3.5	-10.5	
minimum	3.7	96.0	0.1	0.2	0.1						0.3	94.2	0.3	1.4	0.0	-9.3	-13.8	
Fe-DOLOMITE																		
average	26.6	57.3	0.4	15.6	0.0	26.6	56.6	0.6	16.1	0.0						-4.0	-9.2	Patches Fe-dolomite
maximum	31.6	59.7	0.9	18.8	0.1	30.3	59.2	1.4	19.0	0.1						-3.3	-4.6	Occasionally zoned
minimum	23.1	51.8	0.2	12.7	0.0	22.9	54.2	0.3	12.4	0.0						-6.2	-14.2	
ANKERITE																		
average	23.2	52.7	0.8	23.2	0.0	22.9	52.1	0.9	21.1	0.0						-	-	Patches ankerite
maximum	27.5	57.2	1.4	48.7	0.1	25.9	57.1	1.0		0.0						-	-	Occasionally zoned
minimum	20.0	21.9	0.2	19.3	0.0	20.0	51.9	0.7	19.3	0.0								
"T" Sandstone																		
SIDERITE S1																		
average						0.1	2.7	0.1	97.2	0.0	9.5	5.0	1.0	83.4	0.0	-2.7	-4.7	Siderite lens
maximum						0.1	5.2	0.1	99.8	0.0	16.4	8.6	3.9	99.9	0.2	-2.8	-6.3	
minimum						0.0	0.1	0.1	94.5	0.0	0.0	0.0	0.0	71.5	0.0	-2.6	-3.0	
SIDERITE S2																		
average						17.2	7.2	0.4	73.7	0.0						-6.5	-12.4	Rhombic siderite
maximum						33.7	13.0	2.0	94.5	0.1						-9.6	-13.1	Occasionally zoned
minimum						0.1	1.2	0.0	52.5	0.0						-3.4	-11.6	
CALCITE																		
average	0.6	97.2	0.3	1.9	0.0	0.7	96.5	0.6	2.2	0.0	0.8	96.2	0.6	2.4	0.0	-7.7	-10.5	Patches calcite
maximum	0.7	97.5	0.3	2.0	0.1	2.5	98.5	1.6	7.9	0.1	2.5	98.5	1.6	7.9	0.1	-1.3	-6.7	
minimum	0.5	97.0	0.3	1.7	0.0	0.2	89.0	0.1	1.0	0.0	0.2	89.0	0.4	1.0	0.0	-12.7	-11.6	
Fe-DOLOMITE																		
average	26.7	56.0	0.3	17.0	0.0	24.9	57.6	0.4	17.2	0.0						-4.7	-9.4	Fe-dolomite zoned rhombs
maximum	27.7	57.4	0.4	19.0	0.1	27.3	59.0	0.5	19.4	0.0						-3.4	-4.8	reemplacing feldspar
minimum	25.4	54.8	0.2	16.0	0.0	22.5	53.9	0.2	15.5	0.0						-7.1	-13.7	
ANKERITE																		
average	19.6	56.9	0.7	22.8	0.0	18.4	57.6	0.8	23.2	0.0	16.1	57.3	2.1	24.6	0.0	-	-	Patches ankerite
maximum	25.5	59.7	1.0	26.9	0.0	21.2	59.6	1.9	25.8	0.0	17.6	59.2	3.2	25.5	0.0	-	-	Occasionally zoned
minimum	16.7	54.3	0.5	19.7	0.0	15.5	56.2	0.5	19.7	0.0	14.7	55.0	1.3	22.3	0.0	-	-	

"U" SANDSTONE	MARINE + TRANSITIONAL CO_3 Mg	Ca	Mn	Fe	Sr	FLUVIAL CO_3 Mg	Ca	Mn	Fe	Sr
SIDERITE S1 (av)	18.6	11.6	0.9	69.1	0.0	1.4	9.2	0.9	77.5	0.0
SIDERITE S2 (av)	23.8	13.9	0.4	61.8	0.0					
CALCITE (av)	3.8	96.5	0.1	0.5	0.1	1.3	95.4	1.0	2.3	0.0
DOLOMITE (av)	26.6	57.0	0.5	15.9	0.0					
ANKERITE (av)	23.1	52.4	0.9	22.2	0.0					

"T" SANDSTONE	MARINE + TRANSITIONAL CO_3 Mg	Ca	Mn	Fe	Sr	FLUVIAL CO_3 Mg	Ca	Mn	Fe	Sr
SIDERITE S1 (av)	0.1	2.7	0.1	97.2	0.0	9.5	5.0	1.0	83.4	0.0
SIDERITE S2 (av)	17.2	7.2	0.4	73.7	0.0					
CALCITE (av)	0.7	96.9	0.5	2.1	0.0	0.8	96.2	0.6	2.4	0.0
DOLOMITE (av)	25.8	56.8	0.4	17.1	0.0					
ANKERITE (av)	19.0	57.3	0.8	23.0	0.0	16.1	57.3	2.1	24.6	0.0

"U" + "T" Sansdstones	MARINE + TRANSITIONAL CO_3 Mg	Ca	Mn	Fe	Sr	FLUVIAL CO_3 Mg	Ca	Mn	Fe	Sr
SIDERITE S1	9.4	7.2	0.5	83.2	0.0	11.0	7.1	1.0	80.5	0.0
SIDERITE S2	20.5	10.6	0.4	67.8	0.0					
SIDERITE S1+S2	14.9	8.9	0.5	75.5	0.0					
CALCITE (av)	2.2	96.7	0.3	1.3	0.1	1.1	95.8	0.8	2.4	0.0
DOLOMITE (av)	26.2	56.9	0.4	16.5	0.0					
ANKERITE (av)	21.0	54.8	0.8	22.6	0.0	16.1	57.3	2.1	24.6	0.0

"U" + "T" Sansdstones	MARINE + TRANSITIONAL + FLUVIAL CO_3 Mg	Ca	Mn	Fe	Sr
S1 (FLUVIAL, MARINE AND TRANSIT.)	10.2	7.1	0.7	81.8	0.0
TOTAL SIDERITE (S1 + S2)	13.6	8.3	0.6	77.1	0.0

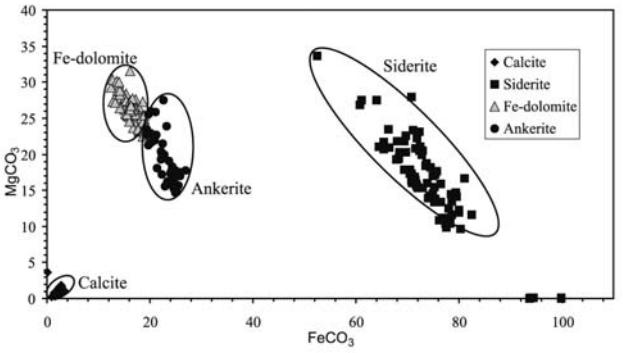

FIGURE 7 | **Plot of magnesium (Mg) and iron contents (Fe) in carbonate cements.**

patches of individual crystals and frequently replaces early siderite (S1) in the transitional and marine sandstones.

Calcite cement postdates quartz overgrowths and chemical compaction. Under SEM, and in BSE mode, quartz and their overgrowths are corroded by this calcite (Fig. 8E), and no chemical zonation was observed. Glauconite is partially or totally replaced by calcite (Figs. 8D and 8F), and pyrite is occluded in this cement (Fig. 8C).

The average composition of the calcite cement in the fluvial environment is ($Ca_{95.8}$ $Fe_{2.4}$ $Mg_{1.1}$ $Mn_{0.8}$) CO_3 (Table 3) and the intergranular volume (IGV) in the sandstones showing calcite cement are 27.7% (Table 1). The average composition of calcite from transitional to marine environment is ($Ca_{96.7}$ $Fe_{1.3}$ $Mg_{2.2}$ $Mn_{0.3}$) CO_3, and the IGV for these sandstones is 13% (Tables 1 and 2). The contents of Mg are < 2 mol % (Figs. 6 and 7) and Sr content varies from below detection limit up to 0.2 mol% (Table 3).

The δ^{13} C values in Napo "U" sandstones vary between -3.5 and -9.3‰, and δ^{18}O from -10.5 to -13.8‰ PDB (Table 3). The δ^{13} C values in "T" sandstones vary between -1.3 and -12.7‰, and δ^{18}O from -6.7 to -11.6‰ PDB (Table 3).

Ferroan dolomite /Ankerite

The Fe-dolomite/ankerite cements are more abundant in the central and the western part of the basin than in eastern part (Fig. 1). These phases replace siderites S1 and enclose S2 (Figs. 9A and 9B). The cements form intergranular mosaics of subeuhedral no luminescent crystals (up to 100 μm), but occasionally they show dispersed patches that corrode quartz and replace feldspars. The percentage of these cements is from 0 to 4% and they post-date quartz overgrowths (Figs. 9C to 9F) and mechanical compaction.

The chemical composition of Fe dolomite in the transitional and marine sandstones (Fig. 1) is ($Mg_{26.2}$ $Fe_{16.5}$ $Mn_{0.4}$ $Ca_{56.9}$) CO_3, and ankerite is ($Mg_{21.}$ $Fe_{22.6}$ $Mn_{0.8}$ $Ca_{54.8}$) CO_3 (Table 3). The average composition of ankerite in the fluvial sandstones is ($Mg_{16.1}$ $Fe_{24.6}$ $Mn_{2.1}$ $Ca_{57.3}$) CO_3 ; Fig. 1). The Fe-dolomite/ankerite displays a patchy zonation in BSE images (Figs. 9C to 9F), which is due to the variations in the $FeCO_3$ content ranging from 12-28 mol % (Figs. 6 and 7). The following isotopic data were obtained for Fe-dolomite and ankerite: δ^{13}C values in Napo "U" sandstones range from -3.3 to -6.2‰, and δ^{18}O from -4.6 to -14.2‰ PDB. The δ^{13} C values in Napo "T" sandstones vary between -3.4 and -7.1‰ and δ^{18}O between -4.8 and -13.7‰ PDB.

POROSITY

The assumed average original porosity is 40% (i.e. moderately to well-sorted sandstones) but varies depending on sorting and cementation. The present porosity of the sandstones is both primary, intergranular porosity, (P1; Fig. 10A) and secondary (P2), with moldic, intergranular and intragranular textural types in minor percentages (Schmidt and McDonald, 1979). Moldic porosity occurs as partial or complete dissolution of feldspars, particularly plagioclase (Fig. 10B). The average porosity (P1+P2) attains a value of approximately 17%, and ranges between 7 and 23%. In most of the samples, there is minor chemical compaction, as grains display long and minor concavo-convex contact.

The maximum reduction of the porosity is 33%. However, in others areas of the basin these values decrease to 14% with respect to the initial porosity. An appreciable primary porosity is preserved by early formation of clay rims (chlorite) that retarded further cementation (Pittman et al., 1992; Ehrenberg, 1993).

The diagram proposed by Houseknecht (1987; Fig. 11A) revealed insignificant impact of compaction compared to cementation in porosity loss. 99% of the data points cluster in the upper right portion of the diagram, indicating that these samples have undergone significant reduction of intergranular volume by cementation processes. The average values for all data are 35% of intergranular volume and 25% cement (Tables 1 and 2). Assuming that the average original porosity of the sandstone was 40%, then 12.5% of the original porosity has been destroyed by compactional processes, whereas 63% has been destroyed by cementation leaving intergranular porosity for all samples at 10%. However, by plotting parameters that take into consideration the reduction in bulk volume due to compaction (Lundergard, 1992), a more realistic evaluation of the relative roles of cementation and compaction is obtained (Fig. 11B). In this diagram some of the samples are plotted in the field of the compactional porosity loss, and the values of intergranular porosity is around 25%.

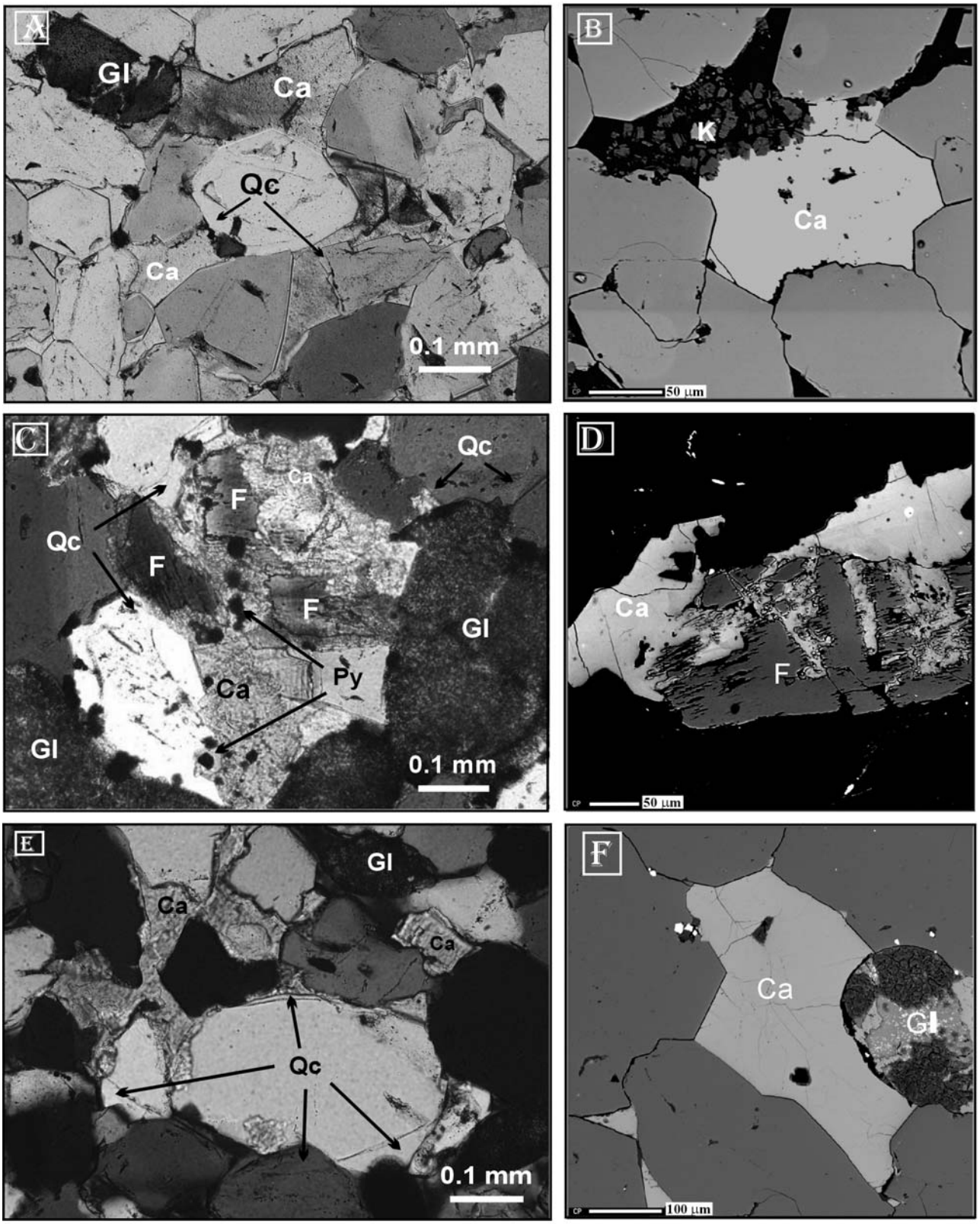

FIGURE 8 | **A) Petrographic aspects of poikilotopic calcite cement, postdating quartz overgrowth in the "U" sandstones. B) Patch of calcite cement postdating quartz overgrowth, corroded by kaolin pore-filling. C) Optical photomicrograph of calcite cement corroding feldspar, glauconite and quartz overgrowth. Pyrite crystals are engulfed in the quartz and carbonate cements. D) BSE image of calcite patches replacing k-feldspar. Note that the calcite and feldspar are partly dissolved. E) Optical photomicrograph of patchy calcite cement corroding quartz overgrowth. F) BSE image of calcite cement post quartz overgrowth. Note glauconite is partially replaced by calcite.**

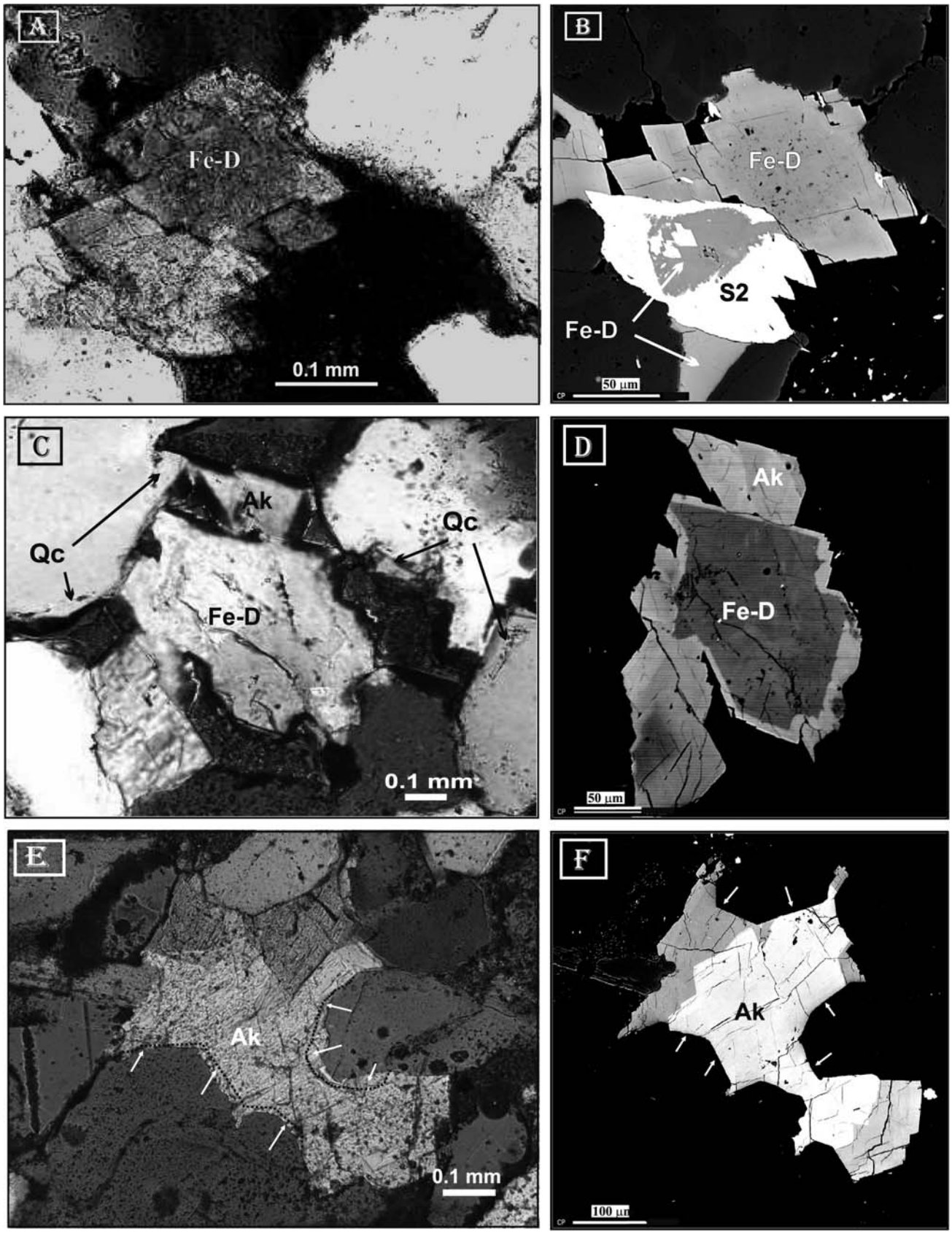

FIGURE 9 | **A and B) Petrographic aspects of Fe-dolomite cements, optical photomicrograph (left), BSE image (right) Rhombohedral Fe-dolomite partially replaced by Mg-siderite (S2). C and D) Mottle aspect of zoned Fe-dolomite cement post quartz overgrowth. The dark core is poor in Fe. E and F) Aspect of patches of zoned ankerite cement post and replacing quart overgrowth (see arrows). Note that in picture F the core is richest in Fe.**

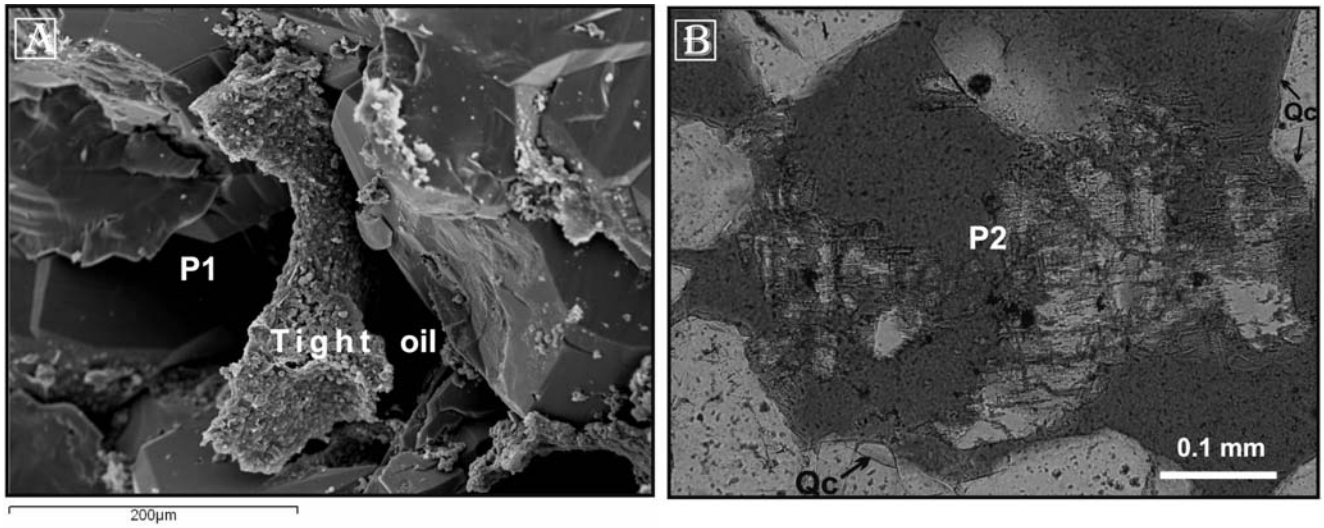

FIGURE 10 | **A) SEM image showing intergranular primary porosity. The amorphous material in the centre of the photo is tight oil (grains up to 200 µm). B) Optical photomicrograph. Petrographic aspect of secondary porosity (intragranular) related to partially dissolved feldspar surrounded by quartz overgrowths (see arrows).**

DISCUSSION

Diagenetic sequence and overall diagenetic evolution of the sandstones

Diagenetic processes in the Cretaceous Napo Fm show that the reservoir sandstones have undergone several changes during burial history. Postdepositional processes caused a significant modification of depositional porosity. The major porosity reducing factors are cementation by quartz, carbonate and clay mineral, as well as the mechanical compaction. Despite the complexity involved in the interpretation of carbonate cementation, owing to the presence of multiple generations and subsequent dissolutions, diagenetic carbonates can provide valuable information regarding the geochemical evolution of the pore waters involved (Morad, 1998). The terms eodiagenesis, mesodiagenesis immature, semi mature and mature stages are used *sensu* Schmidt and McDonald (1979), modified by Morad et al., (2000).

Petrographic and SEM observations, as well as the different intergranular volumes (IGV, in Tables 1 and 2) of the carbonate cemented sandstones, indicated that the cementation is pre-compactional as well as post-compactional. The relative sequence of the main diagenetic processes is presented schematically in Fig. 12. Due to the complex diagenetic pattern and the implicated fluids, the exact timing and origin for certain carbonate phases can not be established. During eodiagenesis, in shallow-water marine facies, a chlorite *clay rim* from a possible early berthierine, was formed beginning at temperature of ≈ 70º (Morad et al., 2000). During this stage thin lens of siderite (S1), and replacements of argillaceous grains and feldspar by this siderite, precipitated in the richest zones of organic matter in both environments. Framboidal pyrite occurred in this stage, appearing in all depositional facies.

The mesogenetic alterations were largely controlled by increases in temperature and by the composition of the diagenetic fluids. In the immature stage, mechanical compaction affected the argillaceous intraclasts, mica, and glauconite grains. In the semimature stage, quartz precipitation started and moderate processes of chemical compaction took place. Quartz cement was postdated by calcite cement in the marine sediments and Fe-dolomite and ankerite cement-replacement in all sandstones. The Fe-dolomite/ankerite phases were replaced by Mg-siderite (S2), which is the last carbonate phase. During the mature stage, at maximum burial depth and related to the organic matter descarboxilation (Smith and McDonald, 1979), siderite (S1, S2), calcite and Fe-dolomite cements were partially dissolved producing secondary porosity (P2). This dissolution event coincided with the beginning of the entries of the hydrocarbon in the Oriente Basin in the Miocene at 8 Ma (Debra, 2001; Dashowood and Abbotts, 1990). Dickite and pyrite-pyrrhotite were the last phase cements after oil entrance in the reservoirs. This diagenetic sequence is similar to the one described in the Lower Cretaceous fluvial and transitional reservoir sandstones in the Salam Field (Egypt´s Western Desert), where well formation temperatures are slightly higher than in the Napo Fm (112ºC to 3,000 m depth; Marfil et al., 2003).

Siderite cement

Siderite cement (S1) was among the first carbonate to precipitate in all the sedimentary environments. In the flu-

vial sandstones, some (S1) siderites have up to 99% $FeCO_3$ and high values in Mn (3.9%; Table 3), suggesting that the siderite cement had precipitated from meteoric fluids, possibly near to the surface water-sediment interphase or in the phreatic zone (Morad et al., 2000; Morad et al., 1998; Mozley, 1989). These authors suggested that siderite richer than 90% $FeCO_3$ and higher than 2.0% $MnCO_3$ indicates an eogenetic process in fluvial environment. However, a Mn-rich siderite was described by Rossi et al. (2001) in the Jurassic reservoir sandstone of Egypt's Western Desert and the high Mg and Ca content was interpreted as precipitated from mixed meteoric and marine water. The thin rhomboidal crystals of (S1 and S2) siderites show chemical zonation, supporting the hypothesis that these cements were formed by precipitations related to the successive changes in the sea level (White et al., 1995), possibly from mixed fluids (Matsumoto and Iijima, 1981; Mozley, 1989; Pye et al., 1990; Moore et al., 1992).

The average composition of the siderite cement (S2) has little differences with respect to the siderite (S1). Siderite (S2) has a higher content of Mg and lower content of Fe and Mn. The chemical values from this mesogenetic siderite cements with high Mg indicates sideroplesite composition (5–30% m $MgC0_3$) (Table 3) (Deer et al., 1962). The Mg could be related to the water enrichment in organic acids (Smith and Ehrenberg, 1989; Morad et al., 2000). Likewise, the increase in the Mg/Fe relation in diagenetic waters formed S2 siderite which could have been caused by the siderite precipitation combined with the increase of the reduction of Fe with depth (Berner, 1980; Canfield, 1989; Fisher and Knipe, 1998). The low values of intergranular volume (19%) indicate that this siderite is post-compactional in origin.

Siderite (S1) precipitated in the early diagenetic phase, possibly due to mica alteration and other argillaceous intraclasts rich in organic matter, as we have observed under optical and fluorescence microscope. The $\delta^{13}C$ ‰ and $\delta^{18}O$ ‰ values for siderite are relatively negatives (Table 3). However, there are two different groups of data that possibly reflect the meteoric origin of S1 with moderate negative values, and S2 with more negative $\delta^{18}O$, indicating mixed meteoric and marine origin or waters modified by diagenetic processes (Fig. 13). The most negative $\delta^{13}C$ values, together with the low $\delta^{18}O$ values, which are interpreted (Irwin et al., 1977; Irwin, 1980; Mozley and Carothers, 1992) as a gradual evolution in the composition of the isotopes during burial, can also be interpreted as related to different origins. Likewise, the most negative $\delta^{18}O$ curves of siderite (-13.1‰ vs V-PDB) and calcite (-13.8‰ vs V-PDB) to cross the shadow area of current formation water (-0.1 to -2.3‰ vs V-SMOW) are just in the present range of temperatures, indicating equilibrium conditions (Fig. 14). This impoverishment in $\delta^{18}O$ of the carbonate cements have been attributes to meteoric incursion (Hudson, 1978; Prosser et al., 1993), to the recrystalization of the cements at higher temperatures (Morad and Eshete, 1990), to Rayleigh fractioning related to the precipitation of early diagenetic minerals (Irwin et al., 1977; Mozley and Carothers, 1992), and to the oxidation of the organic matter in the sulphate reduction zone (Morad and Eshete, 1990). All of these processes could contribute to the lighter oxygen isotopic composition.

Optical microscope and SEM observations show that the S1 siderite maintains the original texture but effectively the major part of the S1 crystals have been

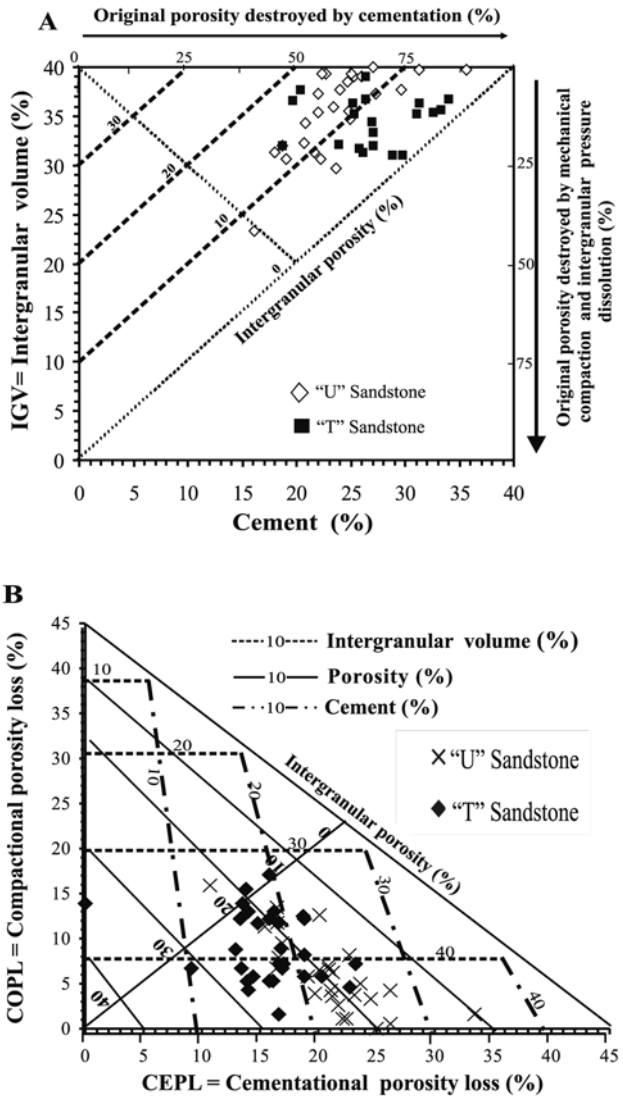

FIGURE 11 | **A) Plot of intergranular volume (%) versus cement (see Houseknecht, 1987). B) Plot of compactional porosity loss (COPL) versus cementation porosity loss (CEPL) (see Lundergard, 1992).**

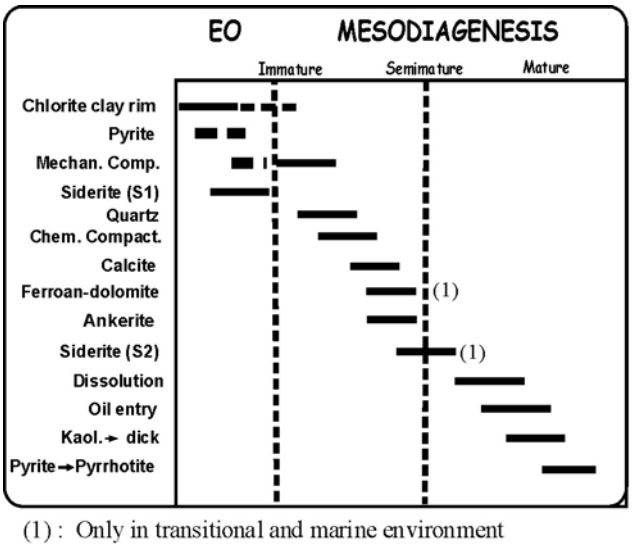

FIGURE 12 | **Paragenetic sequences of the diagenetic processes in the Napo Formation.**

replaced by S2. This argument could justify the low $\delta^{18}O$ of the S2 siderite cement. Moreover, siderite S2 could have precipitated as a result of the thermal descarboxilation of the Mg rich organic matter at temperatures between 80-100ºC. They are slightly lower than the formation temperatures measured in the sampled wells and similar to the temperatures in the North Sea Cretaceous reservoirs (McAulay et al., 1993; Morad, 1998).

Calcite cement

Sandstones cemented by calcite have an average intergranular volume of 24%. This cement postdates quartz cement, suggesting precipitation in a mesogenetic stage (Figs. 8A, 8C, 8E, and 8F). Calcite cement could precipitate from meteoric and marine waters (Fig. 15A). Calcite cement from meteoric and marine waters are relatively pure (96.1% mol de $CaCO_3$) and the Mg + Mn + Fe CO_3 does not exceed 5% mol which is within the range suggested by Boles and Ramseyer, 1987; Ficher and Surdam, 1988; Hayes and Boles 1993; Lee and Boles, 1996. However, the plot of (Fe-Mn-Mg)CO_3 diagram (Fig. 15B) indicates that the majority of the calcite could have precipitated from marine waters according to Lee and Boles diagrams (1996). The high values in Fe could be related to glauconite and mica alterations and the water expelled in the compaction of the intercalated shales in the reservoir sandstones. The source of Ca is not well established, but it can be attributed to the plagioclase alteration (García et al., 1998) or clay minerals in the intercalate shales or limestones (Fig. 2).

The variable low $\delta^{13}C$ and $\delta^{18}O$ values of the calcite cement (Figs.13, 14, and Table 3) suggests that this cement was derived from very different sources and precipitated at different diagenetic temperatures and from different compositional waters. The most negative $\delta^{18}O$ curves of calcite cement (-13.8‰ vs V-PDB) to cross the shadow area of current formation water (-0.1 to -2.3‰ vs V-SMOW) are just in the present range of temperatures, indicating equilibrium conditions (Fig. 14). The most negative values could indicate burial trend in the presence of organic-derived CO_2 (Heydary, 1997) while the less negative values could suggest an evolution from marine waters to modified mesogenetic waters (Hudson, 1978).

Ferroan Dolomite/Ankerite cements

The ferroan dolomite/ankerite cement-replacement precipitated after quartz overgrowth and mechanical and chemical compaction. Optical microscope and BSE show that these carbonates replaced eogenetic siderite (S1) and quartz cement, and in many cases they replaced the feldspars too. The chemical composition of the dolomite and ankerite in the different depositional facies shows no major differences, which suggests that the evolution of the fluid in a thermobaric regime in the basin was mainly ferroan-carbonates precipitated (Galloway, 1984). The high content in Mg and Fe in both cements suggests that the principal sources of solutes for Fe-dolomite-/ankerite precipitation were the sea water, clay minerals, ferromagnesian minerals and the oxidation of sulphides (Curtis and

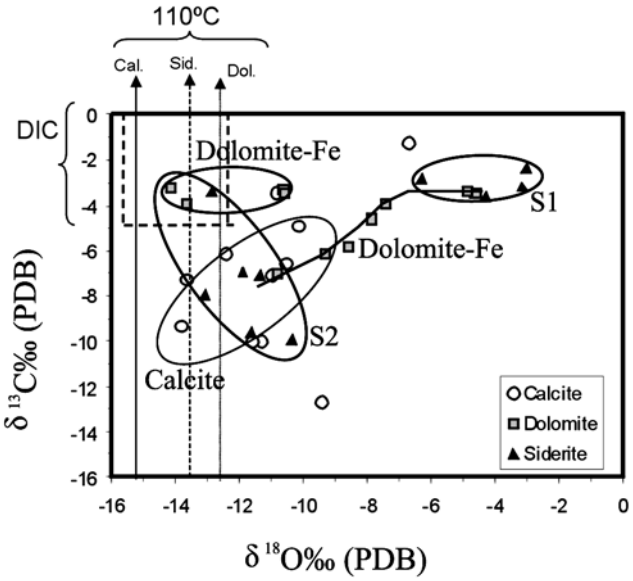

FIGURE 13 | **Isotopic composition of the siderite, calcite and Fe-dolomite cements. Vertical arrows at the left indicate carbonates in equilibrium with present formation water (-1‰ vs V-SMOW) at 110ºC. Present DIC (the dissolved inorganic carbon) of formation water has $\delta^{13}C$ around -4‰ (V-PDB), consequently, present diagenetic processes trend toward $\delta^{18}O$ values are more negatives than -10‰ (V-PDB). The present formation temperature of the bottom hole (110ºC) is represented in the upper part of the diagram.**

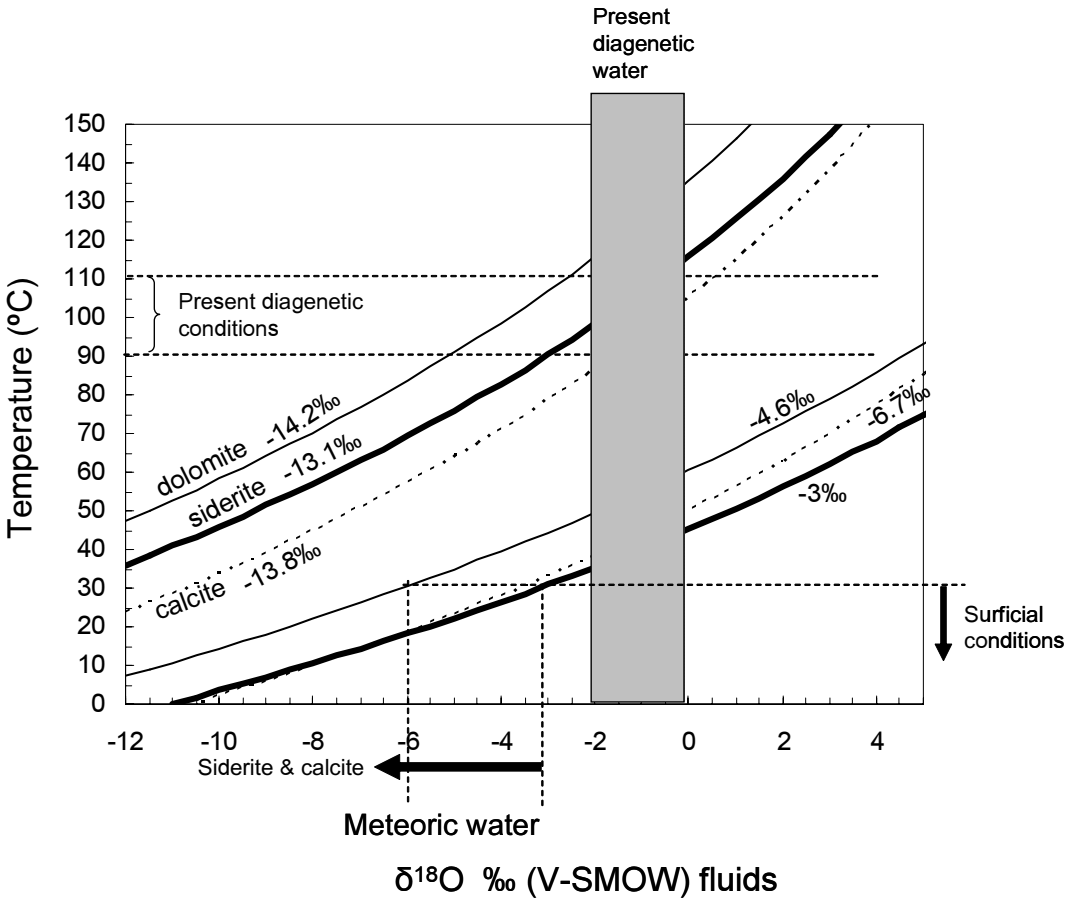

FIGURE 14 | **Diagram showing range of temperature and isotopic composition of the pore fluids constrained for the precipitation of the analyzed calcites, dolomites and siderites. The curves represent the theoretical temperature of carbonates in equilibrium with different waters. Maximum and minimums $\delta^{18}O$ values of siderite, dolomite and calcite have been plotted. The O'Neil et al. (1969), Sheppar and Schwarcz (1970) and Carothers et al. (1988) equations were used to calculate the isotopic fractionation in the systems calcite-water, dolomite-water and siderite-water, respectively.**

Coleman, 1986). These could be justified by the abundance of pyrite and glauconite in the both Napo "T" and "U" sandstones. Although chemical control on the distribution of the siderite and the dolomite-Fe/ankerite has been reported by Matsumoto and Iijima (1981) and Curtis and Coleman (1986), in our case these cements precipitated both in the continental and in the marine sandstones.

The zonation observed in the Fe-dolomite with no corrosion bordering implies that the chemical composition of the fluids was continuously changing and they are attributed to episodic fluctuations in the amounts of dilution of the pore waters. Furthermore, this cement is low in Mn and high in iron content.

The $\delta^{18}O$ values of the Fe-dolomite are negative and show a wide range of values. However, the $\delta^{13}C$ has a narrower range (Table 3 and Fig. 14). Dolomite curve ranging from -14.2 to -4.6‰ vs V-SMOW (Fig. 15) indicates higher temperatures. Likewise, the high content in Fe can explain this apparent increase in temperature and some of the most depleted in $\delta^{18}O$, could have precipitated as consequence of recrystalization of previous carbonates.

The variation in the isotopic composition of the dolomite precipitated in organic matter rich sediments is relatively well documented (Irwin et al., 1977; Mozley and Burns, 1993). The most negative isotopic values of the oxygen in dolomite cements could be related to the continued precipitation at higher temperatures and burial depth, as is supposed by the siderite S2, could have precipitated as a result of the thermal descarboxilation of the Mg rich organic matter and formation temperatures up to 50ºC. The variations in the carbon isotopic composition of the different carbonate cements suggest that rates of organic-carbon oxidation may control the mineralogy of these cements.

CONCLUSIONS

The reservoir sandstones from the Cretaceous Napo Formation in the Oriente Basin were deposited in fluvial,

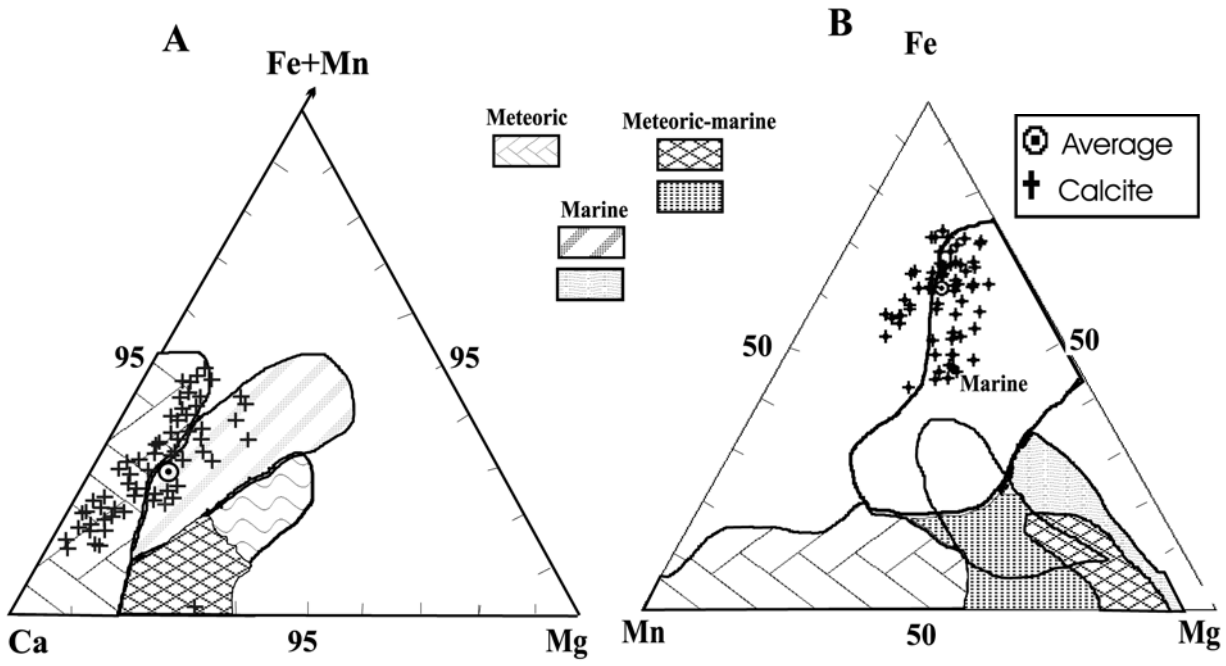

FIGURE 15 | **Calcite composition (mole %) from Napo Formation plotted on the Lee and Boles (1996) diagrams. Compositional fields are distinguished by their inferred diagenetic origin. In (A) calcite precipitated principally from meteoric pore fluids and less samples from mixed marine and meteoric fluids. However, in (B) calcite cement precipitated from marine pore fluids. Beside, many samples are enriched in Fe suggesting that the pore fluids are not related to the depositional fluids and they were enriched in Fe during mesodiagenesis.**

transitional and marine environments. The compositions of these sandstones vary from fine-medium grained quartzarenites (av. $Qt_{96.5}\ F_{3.1}\ RF_{0.4}$) to medium-coarse subarkoses (av. $Qt_{89.8}\ F_{6.8}\ RF_{3.1}$). The principal cements occluding porosity include carbonates, quartz overgrowth, kaolin and subordinated chlorite and pyrite-pyrrhotite. Carbonate cements occur in four mineral phases: eogenetic siderite (S1), mesogenetic and post compaction, calcite, Fe-dolomite as well as ankerite and siderite (S2).

S1 siderite shows high Fe-Ca and low Mn, and occasionally zonation. S2 siderite has high Mg and low Fe and Mn content. The increase in Mg/Fe relation in the diagenetic waters resulted in the precipitation of S2 siderite (sideroplesite). This cement is related to the thermal descarboxilation of the organic matter and the increase of the reduction of Fe with depth. Likewise, the less negative isotopic ratios reflect the meteoric origin of S1. The replacement and recristalization of S1 to S2 siderite could be justified by the low $\delta^{18}O$ ‰ values of some of these carbonate phases.

Fe-dolomite and calcite cements are mesogenetic and post compaction. However, the high Mg and Fe content in the cements and the most negative values of the isotopic data could indicate high temperature and deep burial in the presence of organic derived CO_2, while the less negative values suggest a transition from mixed meteoric and marine waters to modified mesogenetic waters. The moderate to high IGV values and elevated primary porosity permitted the preservation of the isotopic signal of the fluids even during the first stages of burial. However, the high content in Fe and some of the isotopic data point out an unclear origin for some of the calcite and Fe-dolomite cements.

Intergranular volume vs cement show that the cementation process was the diagenetic event that mainly influenced porosity reduction. These reservoir sandstones experienced the loss of some primary porosity at an early stage of diagenesis due to the precipitation of chlorite and siderite S1 cements. However, this early cements helped to retain the porosity delaying the compaction of the sandstone. The high intergranular volume (av. 35%) in the sandstones cemented by S2 siderite and Fe-dolomite-ankerite confirms that these phases precipitated during mesodiagénesis but at shallow burial depth. During the thermal descarboxilation of the organic matter in a later stage of mesodiagenesis, the dissolution of carbonate cements and feldspars was the main mechanisms for secondary porosity development.

Thus, linking diagenesis to the different depositional environments such as fluvial, transitional and shallow marine of siliciclastic sediments has important implications for unravelling and predicting the spatial and temporal distribution of diagenetic alterations and their influence on reservoir quality. The impact of the carbonate cement in the studied reservoirs has positive influence when these cements are

eogenetic, preserving the original primary porosity. However the mesogenetic cements has minor impact in these reservoir, and only secondary porosity occurs when organic acids from interbedded shales circulated at depth.

ACKNOWLEDGEMENTS

This work was partially funded by Project BTE2003-06915 and 01-LEC-EMA 10F of the European Science Foundation, REN2002-11404-E from the Spanish Ministry of Science and Technology. We acknowledge the suggestions and comments made by the reviewers Dr. Anna Travé and Dr. Sadom Morad, and the associate editor Dr. L. Cabrera, which helped to improve the paper.

ACKNOWLEDGEMENTS

Al-Aasm, I.S., Taylor, B.E., South, B., 1990. Stable Isotope analysis of multiple carbonate samples using selective acid extraction. Chemical Geology, 80, 119-125.

Almeida, J.P., 1986. Estudio de litofacies y del contacto agua petróleo de la Arenisca "T" del Campo Libertador. Memoria tomo III: Geología del petróleo Ingeniería de petróleos, 1, 119-148.

Baldock, J.W., 1982. Geología del Ecuador. Boletín de la explicación del mapa geológico de la República del Ecuador. Scale 1:1000.000, 66 pp.

Berner, R.A., 1980. Early Diagenesis: A theoretical Approach. New Jersey, Princeton University Press, 241 pp.

Boles, J.R., Ramseyer, K., 1987. Diagenetic carbonate in Miocene sandstone reservoir, San Joaquin Basin, California. American Association of Petroleum Geologist Bulletin, 71, 1475-1487.

Canfield, D.E., 1989. Reactive iron in Marine sediments. Geochimica and Cosmochimica Acta, 53, 619-632.

Carothers, W.W., Adam, L.H., Rosenbauer, R.J., 1988. Oxygen isotope fractionation between siderite-water and phosphoric acid liberated CO_2-siderite. Geochimica and Cosmochimica Acta, 52, 2445-2450.

Christophoul, F., Rivadeneira, M., 1986. Evaluación Geoquímica de Rocas Madres de la Cuenca Amazónica Ecuatoriana. IV Congreso Ecuatoriano de Geología, Minas y Petróleos, Quito, Ecuador, Colegio de Ingenieros Geólogos de Minas y Petróleos de Pichincha, Memorias, tomo II, 78 pp.

Curtis, C.D., Coleman, M.L., 1986. Controls on the precipitation of early diagenetic calcite, dolomite, and siderite concretions in complex depositional sequences. In: Gautier, D.L. (ed.). Roles of organic matter in sediments diagenesis. Society of Economic Paleontologist and Mineralogist, Special Publication, 38, 23-33.

Dashwood, M.F., Abbotts, I.L., 1990. Aspects of the petroleum geology of the Oriente Basin, Ecuador. In: Brooks, J., (ed.). Classic petroleum provinces. Geological Society, London, Special Publication, 50, 89-117.

Debra, K.H., 2001. The Putumayo-Oriente-Marañon province of Colombia, Ecuador and Peru-Mesozoic-Cenozoic and Paleozoic Petroleum System. U.S. Geological Survey Digital Data Series, 63, 1-35.

Deer, W.A., Howie, R.A., Zussman, J., 1962. Carbonates. In: Deer, W.A., Howie, R.A., Zussman, J., (eds.). Petroleum Geochemistry and exploration of Europe. Oxford, Blackwell, 113-125.

Dott., R.H. Jr., 1964. Wacke Graywacke and matrix - What Approach to Inmature Sandstone Classification. Journal of Sedimentary Petrolology, 34, 625-632.

Ehrenberg, S.N., 1993. Preservation of anomalously high porosity in deeply buried sandstones by grain-coating chlorite: Examples from the Norwegian continental shelf. American Association of Petroleum Geologists, 77, 1260-1286.

Fisher, Q.J., Knipe, R.J., 1998. Microstructural controls on the petrographical properties of deformation properties. In: Jones, G., Fisher, Q.J., Knipe, R.J. (eds.). Faulting and fault sealing in hydrocarbon reservoir. Geological Society, London, Special Publication, 147, 117-134.

Fischer, K.S., Surdam, R.C., 1988. Contrasting diagenetic styles in a shelf turbidite sandstone sequence: The Santa Margarita and Stevens sandstones, San Joaquin Basin, California, USA. In: Graham, A. (ed.). Studies of the Geology of the San Joaquin Basin. Society of Economic Paleontologists and Mineralogists, Pacific Section, 60, 233–247.

Galloway, W.E., 1984. Hydrogeologic regimes of sandstone diagenesis. In: McDonald D.A., Surdam, R.C. (eds.). Clastic diagenesis. American Association of Petroleum Geologist Bulletin, Memoir, 37, 3-13

García, A.J., Morad, S., De Ros, L.F., Al-Aasm, I.S., 1998. Paleogeographical, paleoclimatic and burial history controls on the diagenetic evolution of reservoir sandstone: evidence from the Lower Cretaceous Serraria sandstones in the Sergipe-Alagoas Basin, NE Brazil. In: Morad, S. (ed.). Carbonate cementation in sandstones. International Association of Sedimentology, Special Publication, 26, 107-140.

Hayes M.J., Boles, J.R., 1993. Evidence for meteoric recharge in the San Joaquín Basin, California provided by isotope and trace element chemistry of calcite. Marine and Petroleum Geology, 10, 135-144.

Heydary, E., 1997. Hydrotectonic models of burial diagenesis in platform carbonates based on formation water geochemistry in North American sedimentary basins. Society of Economic Paleontologist and Mineralogist (SEPM), Special Publication, 57, 53-79.

Houseknecht, D.W., 1987. Assessing the relative importance on compaction processes and cementation to reduction of porosity in sandstones. American Association of Petroleum Geologist, Bulletin, 71, 633-642.

Hudson, J.D., 1978. Carbon isotopes and limestone cements. Geology, 3, 19-22.

Irwin, H., 1980. Early diagenetic carbonate precipitation and pore-fluid migration in the Kimmeridge Clay of Dorset, England. Sedimentology, 27, 577-597.

Irwin, H., Curtis, Ch., Coleman, M., 1977. Isotope evidence for several sources of diagenetic carbonates formed during burial of organic-rich sediments. Nature, 269, 209-213.

Jaillard, E., 1997. Síntesis estratigráfica y sedimentológica del Cretácico y Paleógeno de la Cuenca Oriental del Ecuador. Informe final Convenio Orstom-Petroproduccion, 1, 164 pp.

Lee, Y., Boles, J.R., 1996. Depositional control on carbonate cement in the San Joaquin Basin, California. Siliciclastic diagenesis and fluid flow: Concepts and applications. Society of Economic Paleontologists and Mineralogists (SEPM), Special Publication, 55, 13-22.

Lundergard, P.D., 1992. Sandstone porosity loss—a "big picture" view of the importance of compaction. Journal of Sedimentary Petrology, 62, 250-260.

Matsumoto, R., Iijima A., 1981. Origin and diagenetic evolution of Ca-Mg-Fe carbonates in some coalfields of Japan. International Association of Sedimentologist, 28, 239-259.

Marfil, R., Delgado A., Rossi C., La Iglesia, A., Ramseyer, K., 2003. Origin and diagenetic evolution of Kaolin in reservoir sandstone and associated shales of Jurassic and Cretaceous Salam Fields, Western Desert (Egypt). In Worden, R.H., Morad, S. (eds.). Clay Mineral Cements in Sandstone. International Association Sedimentologist, Special Publication, 34, 319-342.

McAulay, G.E., Burley, S.D., Johnes, L.H., 1993. Silicate mineral authigenesis in the Hutton and NW Hutton fields: Implications for sub-surface porosity development. In: Parker, J.R. (ed.). Petroleum Geology of Northwest Europe. Proceedings of the 4th Conference. The Geological Society of London, London, 1377-1394.

Moore, S.E., Ferrell, R.E., Aharon, P., 1992. Diagenetic siderite and other Ferroan carbonates in a modern subsiding marsh sequence. Journal Sedimentary Petrology, 62, 537-366.

Morad, S., 1998. Carbonate cementation in sandstone: distribution patterns and geochemical evolution. International Association Sedimentologist, Special Publication, 26, 1-26.

Morad, S., Eshete, M., 1990. Petrology, chemistry and diagénesis of calcite concretions in Silurian shale from central Sweden. Sedimentary Geology, 66, 113-134.

Morad, S., Ketzer, J.M., De Ross, L.F., 2000. Spatial and temporal Distribution of diagenesis alteration in siliciclastic rocks: implications for mass transfer in sedimentary basin. Sedimentology, 47, 95-120.

Mozley, P.S., 1989. Relation between depositional environment and the elemental composition of early diagenetic siderite. Geology, 17, 704-706.

Mozley, P.S., Carothers, W.W., 1992. Elemental and isotopic composition of siderite in the Kuparuk Formation, Alaska: Effect of microbial activity and water sediment interaction on early pore water chemistry. Journal of Sedimentary Petrology, 62, 681-692

Mozley, P.S., Burns, S.J., 1993. Oxygen and carbon isotopic composition of marine carbonate concretions: An overview. Journal of Sedimentary Petrology, 63, 73-83.

O'Neil, J.R., Clayton, R.N., Mayeda, T.K., 1969. Oxygen isotope fractionation in divalent metal carbonates. Journal of Chemical Physics, 51, 5547-5558.

Pettijohn, F.J., Potter, P.E., Siever, R., 1972. Sand and sandstone. New York, Springer-Verlag, 618 pp.

Pittman, E.D., Larese, R.E., Heald, H.T., 1992. Clay coats: Occurrence and relevance to preservation of porosity in sandstones. In: Houseknecht, D.W., Pittman, E.D. (eds.). Origin, Diagenesis, and Petrophysics of Clay Minerals in Sandstones. Society of Economic Paleontologists and Mineralogist, Special Publication, 47, 241-255.

Prosser, D.J., Daws, J.A, Fallick, A.E., Williams, B.P.J., 1993. Geochemistry and diagenesis of stratabound calcite cement layers within the Rannoch Formation of the Brent Group, Murchinson, Field North Viking Graben (Northern Nort Sea). Sedimentary Geology, 87, 139-164.

Pye, K., Dickinson, J.A.D., Schiavon, N., Coleman, M.L., Cox, M., 1990. Formation of siderite-Mg-calcite-iron sulphide concretions in intertital marsh and sandflat sediments, North Norfolk, England. Sedimentology, 37, 325-343.

Rossi, C., Marfil, R., Ramseyer, K., Permanyer, A., 2001. Facies-Related diagenesis and multiphase siderite cementation and dissolution in the reservoir sandstones of the Khatatba Formation, Egyipt's Western Desert. Journal of Sedimentary Research, 71, 459-472.

Schmidt, V., McDonald, D.A., 1979. The role of secondary porosity in the course of sandstone diagenesis. In: Scholle, A., Schluger, P.R. (eds.). Aspect of diagenesis. Society of Economic Paleontologists and Mineralogist, Special Publication, 26, 175-207.

Sheppard, S.M.F., Schwarcz, E., 1970. D/H and $^{18}O/^{16}O$ ratios of minerals of possible mantle or lower crustal origin. Earth and Planetary Science Letters, 9, 232-239

Smith, J.T., Ehrenberg, S.N., 1989. Correlation of carbon dioxide abundances with temperature in clastic hydrocarbon reservoir: relationship to inorganic chemical equilibrium. Marine and Petroleum Geology, 6, 129-135

White, H.J., Skopec, R., Ramirez, F., Rodas, J., Bonilla, G., 1995. Reservoir characteristics of Hollín and Napo Formations, western Oriente basin, Ecuador. In: Tankard, A.J., Suárez, S.R., Welsink, H.J. (eds.). Petroleum basin of South America. American Association of Petroleum Geologist, Memoir, 62, 573-596.

Manuscript received January 2005;
revision accepted July 2006.